

Epitaxial-strain-induced multiferroicity in SrMnO₃ from first principles

Jun Hee Lee* and Karin M. Rabe

Department of Physics and Astronomy, Rutgers University, Piscataway, New Jersey 08854-8019, USA

First-principles density-functional calculations reveal a large spin-phonon coupling in cubic SrMnO₃, with ferromagnetic ordering producing a polar instability. Through combination of this coupling with the strain-polarization coupling characteristic of perovskites, the bulk antiferromagnetic paraelectric ground state of SrMnO₃ is shown to be driven to a previously unreported multiferroic ferroelectric-ferromagnetic state by increasing epitaxial strain, both tensile and compressive. This state has a computed polarization and estimated Curie temperature above 54 $\mu\text{C}/\text{cm}^2$ and 92 K. Large mixed magnetic-electric-elastic responses are predicted in the vicinity of the phase boundaries.

PACS numbers: 75.80.+q, 63.20.-e, 75.10.Hk, 77.80.-e

Multiferroic materials have been the subject of continuing attention both for fundamental physics and for potential applications including transducers and information storage [1, 2, 3]. There is particular interest in the search for multiferroic materials with large polarization ($P > 1\mu\text{C}/\text{cm}^2$) and magnetization that persists to high temperatures, as well as a strong coupling between the magnetism and the electric polarization. This coupling may be enhanced by proximity of the system to a morphotropic phase boundary.

With epitaxial strain, it is possible to widen the search to include phases and phase boundaries that do not appear in bulk. In many paraelectric perovskite oxides, epitaxial strain couples strongly to the lowest-frequency polar phonon; this is responsible for the phenomenon of epitaxial-strain-induced ferroelectricity, which has been intensively studied both experimentally and theoretically [4, 5, 6]. In an antiferromagnetic-paraelectric system, there is a further intriguing possibility. If the system has a spin-phonon coupling in which the lowest-frequency polar phonon is softer for ferromagnetic ordering than for antiferromagnetic ordering, then epitaxial strain enhancement of a polar instability lead to the lowering of the energy of the ferromagnetic (FM)-ferroelectric (FE) state below that of the antiferromagnetic (AFM)-paraelectric (PE) state. This mechanism for producing a multiferroic phase was proposed and elucidated using first-principles calculations for EuTiO₃ [7], with polarization above 30 $\mu\text{C}/\text{cm}^2$) at -2.0 % strain but a low Curie temperature comparable to the bulk Neel temperature of 5.5 K [8].

The demonstration of the spin-phonon coupling mechanism for epitaxial-strain-induced multiferroicity in EuTiO₃ suggests a search for other paraelectric antiferromagnetic materials in which this mechanism could be realized and the performance optimized. The primary criterion is that of a large downward shift in the frequency of the lowest polar phonon with ferromagnetic ordering, which leads to a large energy gain for polar distortion of the ferromagnetic state. Next, we look for systems with a moderate Neel temperature (T_N): while it would be

preferable to have the magnetic ordering temperatures as high as possible, this is limited by the fact that the FM-AFM energy splitting cannot be larger than the scale of the energy gain for polar distortion of the ferromagnetic state. Finally, the polar instability should be strong enough to compete with any other structural distortions, such as oxygen octahedron rotations.

B-site magnetic perovskite oxides are of particular interest, as the larger exchange coupling results in much higher magnetic ordering temperatures than that of *A*-site rare-earth systems such as EuTiO₃. Perovskite manganites are especially promising as they show strong magnetoelectronic and magnetostructural effects, including colossal magnetoresistance [9] and magnetic-field-induced structural transitions [10]. Indeed, a first-principles survey of the phonon dispersions of cubic perovskite oxides, including previously reported results on chromites [11] and our own investigations of chromites, ferrites and manganites compounds [12] shows strong spin-phonon coupling in both SrMnO₃ and CaMnO₃. Though both compounds have moderate a moderate T_N , we focus on SrMnO₃ as the strong oxygen octahedron instabilities in CaMnO₃ are less favorable for realization of the spin-phonon mechanism.

In this paper, we report first-principles observation of strong spin-phonon coupling and a resulting epitaxial strain induced multiferroic phase in SrMnO₃ (SMO), a AFM-PE d^3 perovskite oxide. In bulk, SMO is observed to have *G*-type antiferromagnetic ordering at $T_N \approx 233$ -260 K in the cubic perovskite structure [13, 14]. In the *G*-AFM phase, we find the epitaxial-strain-induced ferroelectricity previously suggested in Ref. 15. Further, we find that the polar instability is strongly coupled to ferromagnetic ordering. Thus, the increase in polarization produced by increasing tensile strain leads to additional magnetic transitions, first to *C*-AFM and then to *A*-AFM ordering, with an increasing fraction of parallel nearest neighbor Mn spins, before the final transition to the ferroelectric FM phase. For compressive strain, the transition occurs directly from the *G*-AFM to the ferroelectric FM phase. While the cubic FM phase is metal-

TABLE I: Calculated lowest phonon frequencies, in cm^{-1} , of cubic SrMnO_3 at calculated equilibrium lattice constants with G -AFM and FM orderings for high symmetry q -points.

	Γ	X	R	M
G -AFM ($a_0=3.845\text{\AA}$)	121	116	$84.5i$	$38.1i$
FM ($a_0=3.845\text{\AA}$)	$76.2i$	116	$114i$	$86.3i$
FM ($a_0=3.865\text{\AA}$)	$109i$	113	$119i$	$89.9i$

lic, in both cases, the system with the equilibrium polar distortion is insulating. Finally, we predict large mixed magnetic-electric-elastic responses in the vicinity of the phase boundaries.

First-principles calculations were performed using density-functional theory within the generalized gradient approximation GGA+ U method with the Perdew-Becke-Erzenhof parametrization [16] as implemented in the *Vienna Ab Initio Simulation Package* (VASP-4.6) [17, 18]; selected LSDA+ U calculations were performed for comparison. We use the Dudarev [19] implementation with on-site Coulomb interaction $U=2.7$ eV and on-site exchange interaction $J_H=1$ eV to treat the localized d electron states in Mn. Within GGA+ U , this choice gives agreement between the calculated ($2.7\mu_B$) and experimental magnetic moments ($2.6\mu_B\pm 0.2$) [14] and is similar to that in a previous GGA+ U study [20]. The projector augmented wave (PAW) potentials [21] explicitly include 10 valence electrons for Sr ($3s23p64s2$), 13 for Mn ($3p63d54s2$), and 6 for oxygen ($2s22p4$).

The phonon frequencies of the ideal cubic perovskite G -AFM and FM reference structures were computed using the frozen phonon method in a $\sqrt{2}\times\sqrt{2}\times 2$ supercell with a $6\times 6\times 4$ Monkhorst-Pack (M-P) k -point mesh at the Γ , R, X and M points of the primitive perovskite Brillouin zone; as spin-orbit coupling was not included, these wavevectors remained good quantum numbers for both FM and G -AFM orderings.

To find the minimum-energy configuration in a given space group determined by freezing in one or more unstable modes of the cubic reference structure, we moved the atoms according to the conjugate-gradient algorithm until the residual Hellman-Feynman forces were less than $1.0\text{meV}/\text{\AA}$. Structural optimizations were performed for 20-atom $\sqrt{2}\times\sqrt{2}\times 2$ with a $4\times 4\times 4$ M-P k -point mesh; for A -AFM $R_4^+[110]+\Gamma_4^-[110]$, a $2\times 2\times 2$ supercell with a $4\times 4\times 4$ M-P k -point mesh was used.

To study the effects of epitaxial strain, we performed ‘‘strained-bulk’’ calculations [22] in which calculations were performed for the periodic crystal with appropriate epitaxial constraints imposed on the in-plane lattice parameters, with all atomic positions and the out-of-plane lattice constant optimized. Epitaxial strain is here defined relative to the computed lattice constant for the G -AFM cubic perovskite structure (3.845\AA). Ferroelec-

tric polarizations for the relaxed structures at each strain were computed by the Berry-phase method [23]. Curie and Neel temperatures for a given strain are estimated from the energy differences between FM and G , C and A -AFM orderings assuming two exchange constants (in-plane and out-of-plane nearest neighbor couplings) and applying mean field theory [24]. As exchange couplings are generally overestimated in DFT, to obtain a prediction useful for quantitative comparison with experiment, we then uniformly rescaled the temperature so that the energy difference for the bulk cubic perovskite phase ($\Delta E=86\text{meV}$, $T_{N,MFT}=3300\text{K}$) corresponds to the experimental value of $T_N=250\text{K}$ [13, 14].

The calculated lattice constants of cubic G -AFM and FM SrMnO_3 are $a=3.845\text{\AA}$ and 3.865\AA , respectively; the slight overestimate relative to the experimental G -AFM value $a=3.80\text{\AA}$ [13, 14] is typical of GGA calculations for oxides. The computed lowest phonon frequencies of cubic FM and G -AFM SrMnO_3 at the computed lattice constant for the cubic G -AFM structure are shown in Tab. I; for the cubic FM structure, the computed lattice constant is very similar and the effect of the difference on the phonon frequency, also is given in Table I, is small except at Γ . The unstable modes at the M and R points are the oxygen octahedron rotations. Across the Brillouin zone, the FM modes are lower in frequency than the corresponding modes in the G -AFM structure. This effect is especially dramatic at Γ , where the lowest frequency TO mode is stable in the G -AFM structure but unstable in the FM structure. The corresponding eigenvectors are $(\text{Sr},\text{Mn},\text{O}_{\parallel},\text{O}_{\perp}) = (0.10,0.31,-0.52,-0.56)$ for G -AFM and $(0.03,0.41,-0.42,-0.57)$ for FM, showing displacement of both the Sr and Mn cations relative to a fairly rigid oxygen octahedral network.

From the presence of unstable modes, it is clear that the computed ground state of SrMnO_3 is not the ideal cubic perovskite structure. However, the energy gains and distortions for the G -AFM structure resulting from freezing in the dominant M_3^+ and/or R_4^+ unstable modes are quite small. For example, the equilibrium $R_4^+[001]$ rotation angle is 4.8° , resulting in a $I4/mcm$ structure with an energy 6.2 meV/f.u. lower than the ideal cubic perovskite structure. $R\bar{3}c(R_4^+[111])$ and $Imma(R_4^+[110])$ yield similar equilibrium angles and energy gains, while $P4/mbm(M_3^+[001])$ is smaller still, with 2.4° and energy gain 0.4 meV/f.u. This is consistent with the experimental observation that AFM SrMnO_3 has a cubic structure but transforms to the $I4/mcm$ structure with a small fraction of A -site substitution by the smaller cation Ca [13]. For FM ordering, the energy of the equilibrium cubic structure is 76 meV/f.u. higher than that of the G -AFM cubic structure, and all FM structures are higher in energy than the lowest-energy AFM structure, despite the lower frequencies of the M, R and Γ modes and larger relaxation energies.

The restrictions on lattice vectors at 0% epitaxial

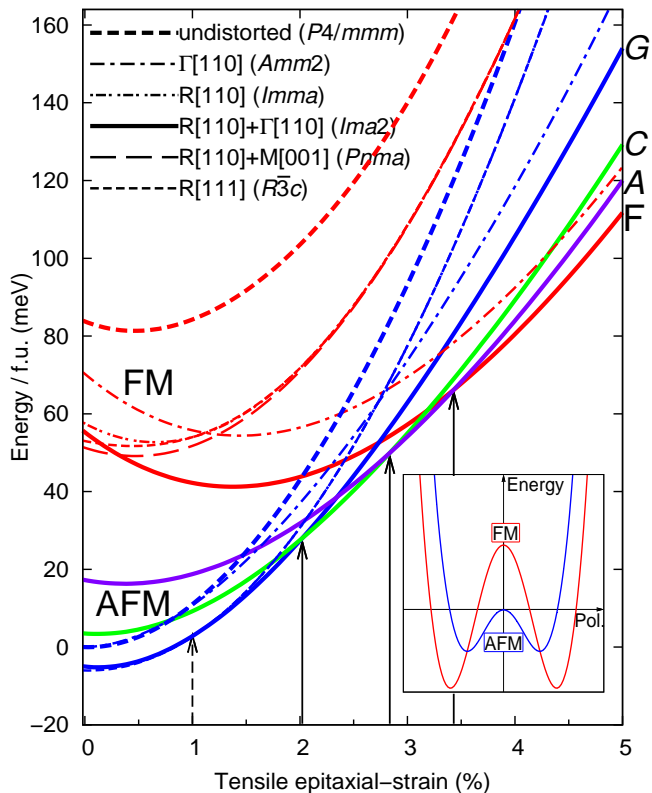


FIG. 1: (Color online) GGA+ U total energies of various structures, per formula unit, obtained by freezing in the given mode(s). Calculations were performed at integer values of strain and interpolated. The energies of structures with FM ordering are shown in red, for G -AFM in blue, C -AFM in green and A -AFM in violet. Vertical black dotted lines at 1.0%, 2.0%, 2.8% and 3.4% strain indicate phase boundaries separating $Imma$ (G -AFM), $Ima2$ (G -AFM), $Ima2$ (C -AFM), $Ima2$ (A -AFM) and $Ima2$ (FM) states. The inset is a schematic showing the stability of the FM-FE state at large strain.

strain change these distortions and energy differences only slightly; the results for the latter are included in Figure 1. For example, the tetragonal relaxation of the FM state lowers its energy slightly, so that the AFM-FM splitting is 84 meV/f.u. For the $R_4^+[001]$ rotation, the equilibrium angle is almost the same (4.7°) and the energy lowering is slightly smaller (5.4 meV/f.u.).

In Fig. 1, the epitaxial strain dependence of the total energies of various structures and magnetic orderings is shown for tensile strain from 0% to 5%. The energies of the G -AFM phases are seen to increase with increasing tensile strain. Because of their coupling to strain, the lowest frequency polar modes in the G -AFM $P4/mmm$ and $Imma$ ($R_4^+[110]$) structures become unstable at a critical strain of about 1%, with second-order phase transitions to the polar $Amm2$ ($\Gamma_4^-[110]$) and $Ima2$ ($R_4^+[110]+\Gamma_4^-[110]$) phases, respectively. The polar distortion and associated energy gain increase with increasing strain. This epitaxial-strain-induced

ferroelectricity in the antiferromagnetic state is analogous to that previously found in nonmagnetic $P4/mmm$ SrTiO₃[4, 5], $Pnma$ CaTiO₃ [6] and antiferromagnetic $Pnma$ CaMnO₃ [15], with critical strains of 0.6%, 2%, and 2% respectively; hypothetical antiferromagnetic cubic BaMnO₃ [25] is already ferroelectric at its equilibrium lattice constant. The dependence of the total energies on compressive strain, not shown, produces an analogous effect at -2.9% strain

Here, we focus instead on the interplay of the strain and polar instability with the magnetic ordering. In contrast to the AFM phases, the energy of FM structures initially decreases with increasing tensile strains (Fig. 1); this corresponds to the slightly larger computed lattice constant for FM ordering in the undistorted cubic structure. The polar instability leads to a substantial energy lowering which increases with increasing strain, so that at tensile strains above 3.4% the energy of the $Ima2$ FE-FM structure drops below those of the AFM-FE phases (see inset); for compressive strains, the FE-FM structure with space group $I4cm$ ($R_4^+[001]+\Gamma_4^-[001]$) is favored above a critical strain of -2.9%. The polar distortion with strain also drives a metal-insulator transition above a critical amplitude; at all strains considered, the FE-FM phase is insulating, with a band gap ranging from 0.22 eV at 0% strain to 0.51 eV at 5% strain.

In addition to G -AFM ordering, we also considered $R_4^+[110]+\Gamma_4^-[110]$ phases with C -AFM and A -AFM orderings, in which some fraction of nearest neighbor Mn moments are parallel. Though higher in energy than G -AFM at 0% strain, they are favored by increasing tensile strain. As can be seen in Fig. 1, the polar C -AFM phase, with 1/3 parallel-spin bonds, drops below G -AFM at 2%, and the A -AFM phase drops with 2/3 parallel-spin bonds below the C -AFM phase at 2.8%. For compressive strain, however, the distorted G -AFM state is lower in energy than the A and C states up to the strain where the FM state becomes lower in energy, and thus there are no intermediate transitions.

There are thus four phase transitions in the range of tensile strain considered: G -AFM-PE \rightarrow G -AFM-FE \rightarrow C -AFM-FE \rightarrow A -AFM-FE \rightarrow FM-FE. The strain dependence of the electric polarization and of the estimated Neel (for AFM phases) and Curie (for the FM phase) temperatures are shown in Fig. 2. The three first-order magnetic transitions are of particular interest. At each of these, the change in magnetic order is accompanied by a change in the magnitude of the electric polarization. The magnitude of the polarization change makes typical electric energies ($P \cdot E = 10 \mu\text{C}/\text{cm}^2 \cdot 50 \text{ kV}/\text{cm} = 0.2 \text{ meV}/\text{f.u.}$) comparable to typical magnetic energies ($M \cdot H = 3 \mu_B \cdot 1\text{T} = 0.2 \text{ meV}/\text{f.u.}$). Thus, near the A -AFM-FE \rightarrow FE-FM phase boundary, an applied electric field can induce a nonzero magnetization. A substantial magnetodielectric coupling is also expected at that phase boundary as a magnetic field induced transition to the FM phase will

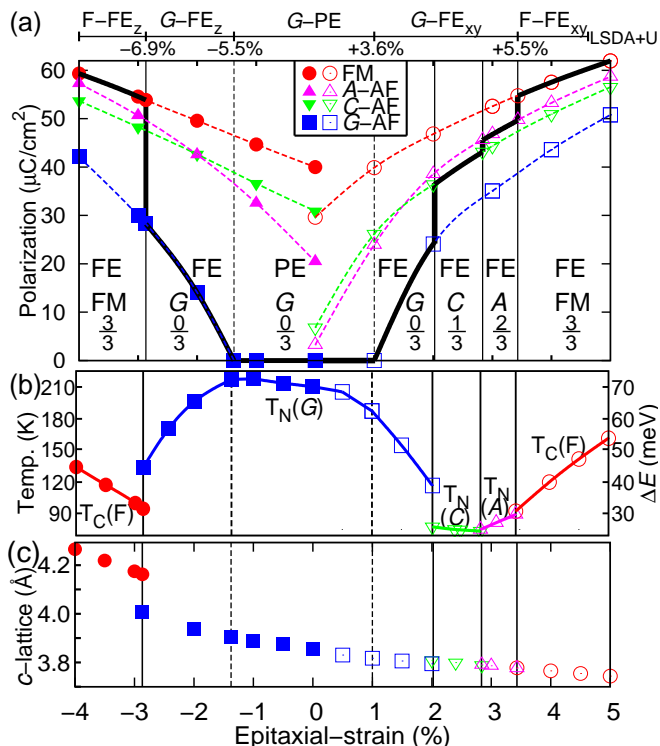


FIG. 2: (Color online) (a) Computed ferroelectric polarization and magnetic transition temperature of SrMnO₃ *G*-AFM (square), *C*-AFM (down triangle), *A*-AFM (up triangle) and FM (circle) in the lowest energy structure at each strain value. The fractions of parallel nearest neighbor spins in each state are given. The bold black line follows the polarization of the lowest energy structure with changing strain. The linear phase diagram at the top, not on the same scale, shows the phases and phase boundaries as computed within LSDA+*U* for comparison. Open and solid symbols represent structures where R rotation is along [110] and [001] respectively. (b) Magnetic ordering temperatures were estimated from computed values of ΔE as described in the text. (c) *c* lattice parameter for the lowest energy structure at each strain value.

also lead to a jump in the FE polarization and in the dielectric constant. At the AFM-FE/FM-FE phase boundary for compressive strain, in addition to an analogous magnetodielectric coupling, a strong strain response is expected due to the jump in *c* lattice parameter.

As discussed above, this mechanism for epitaxial stabilization of a FM-FE phase based on spin-phonon coupling was first discussed for EuTiO₃ [7]. In that system, the polar phonons for the bulk cubic phases are stable, with the phonon in the higher-energy FM phase about 10 cm⁻¹ lower in frequency than that in the *G*-AFM phase. In contrast, in SrMnO₃ at 0% strain both the FM-AFM energy difference and the FM-AFM difference in polar phonon frequency are much greater, the FM polar phonon being unstable. As a result, the metastable FM-FE structure is already present at 0% strain, though the electric field needed to induce this state is inaccessibly high. As in EuTiO₃, strain acts both to increase the fer-

roelectric instability in both phases and to lower the FM-AFM energy splitting. This is apparent in the lowering of *T_N* for *G*-AFM as the phase boundaries are approached, and in the increase of *T_C* with increasing magnitude of strain. The scale of the magnetic ordering temperatures at the phase boundaries is set by the coupling of the magnetic energy splitting to the discontinuous change in structure as the boundary is crossed; this coupling is so strong that the magnetic ordering temperatures remain above 92 K throughout the strain range considered, even at boundaries where the structural discontinuity is relatively small. This offers operating temperatures higher than that of EuTiO₃ [8] and magnetically-driven ferroelectrics [26, 27].

In GGA+*U*, the overestimate of the cell volume may lead to a spurious enhancement of the polar instability. We have investigated this effect by performing calculations for the four lowest-energy phases with LSDA+*U*, where the underestimate of the volume is expected to lead to a comparable suppression of the polar instability. As can be seen from the linear phase diagram at the top of Fig. 2, epitaxial-strain-induced ferroelectricity in the *G*-AFM phase moves to larger strain, and the relative stability of the *C*-AFM and *A*-AFM phases decreases, so that the transition from *G*-AFM-FE to FM-FE occurs at a higher critical strain of 5.5%, which can be regarded as an upper bound. We thus estimate the critical *s* for the FM-FE phase to be $+4.5 \pm 1\%$ (tensile strain), and $-4.9 \pm 2\%$ (compressive strain).

It is well known that changes in the choice of the parameter *U* can have a significant effect on magnetic ordering energies; this was shown in particular in EuTiO₃ [7]. We have verified that the epitaxial-strain-induced multiferroicity occurs for a wide range of possible choices of *U*, though the quantitative details change. For example, use of a slightly larger value of *U* reduces the energy difference between FM and AFM phases while leaving the spin-phonon coupling relatively unchanged so that the critical strain for the FM-FE phase shifts down from 3.4%.

The critical strain for observation of the FM-FE phase in SrMnO₃ is rather high, which may make experimental confirmation challenging. Observation of the behavior characteristic of lower strains, such as the strain-induced ferroelectricity in *G*-AFM and the decrease in *T_N* in the *G*-AFM PE and FE phases, should be taken as indicators of the impending transition to the FM-FE phase at higher strain.

In summary, we have presented first-principles density-functional calculations that reveal a large spin-phonon coupling in cubic SrMnO₃, with ferromagnetic ordering producing a polar instability. Through combination of this coupling with the polarization-strain coupling characteristic of perovskite oxides, both tensile and compressive epitaxial strain drive the system through a series of phase transitions to a ferromagnetic-ferroelectric mul-

tiferroic state. As the magnetic transitions are accompanied by a jump in electric polarization, there is the possibility of electric field control of magnetic ordering; at the two boundaries between AFM and FM phases, the polarization can conversely be controlled by an applied magnetic field. At this boundary for compressive strain, the jump in c lattice parameter also should yield a strong strain response to applied fields. Though the cubic FM phase is metallic, the polar distortion opens a gap in the electronic density of states, resulting in the insulating character of the FM-FE phase. This suggests that the search for epitaxial-strain-induced multiferroics could be productively extended to include other systems with metallic character for the FM reference state.

We thank C.-J. Eklund, C. J. Fennie, V. Gopalan, D. R. Hamann, A. Malashevich, L. Palova, J. Rondinelli, D. Schlom, N. Spaldin, and D. Vanderbilt for valuable discussions. This work was supported by MURI-ARO Grant W911NF-07-1-0410 and ONR Grant N0014-00-1-0261. Part of this work was carried out at the Aspen Center for Physics.

* Electronic address: jhlee@physics.rutgers.edu

- [1] N. A. Spaldin and M. Fiebig, *Science* **309**, 391 (2005).
- [2] R. Ramesh and N. A. Spaldin, *Nature Materials* **6**, 21 (2007).
- [3] S. W. Cheong and M. Mostovoy, *Nature Materials* **6**, 13 (2007).
- [4] J. H. Haeni *et al.*, *Nature (London)* **430**, 758 (2004).
- [5] A. Antons, J. B. Neaton, K. M. Rabe, and D. H. Vanderbilt, *Phys. Rev. B* **71**, 024102 (2005).
- [6] C.-J. Eklund, C. J. Fennie, and K. M. Rabe, *Phys. Rev. B* **79**, 220101(R) (2009).
- [7] C. J. Fennie and K. M. Rabe, *Phys. Rev. Lett.* **97**, 267602 (2006); *ibid.*, unpublished.
- [8] T. Katsufuji and H. Takagi, *Phys. Rev. B* **64**, 054415 (2001).
- [9] A. P. Ramirez, *J. Phys. Cond. Matt.* **9**, 8171 (1997).
- [10] A. Asamitsu, Y. Moritomo, Y. Tomioka, T. Arima and Y. Tokura, *Nature* **373**, 407 (1995).
- [11] N. Ray and U. V. Waghmare, *Phys. Rev. B* **77**, 134112 (2008).
- [12] J. H. Lee and K. M. Rabe (in preparation).
- [13] O. Chmaissem *et al.*, *Phys. Rev. B* **64**, 134412 (2001).
- [14] T. Takeda and S. Ohara, *J. Phys. Soc. Jpn* **37**, 275 (1974).
- [15] S. Bhattacharjee, E. Bousquet, and Ph. Ghosez, *Phys. Rev. Lett.* **102**, 117602 (2009).
- [16] J. P. Perdew, K. Burke, and M. Ernzerhof, *Phys. Rev. Lett.* **77**, 3865 (1996).
- [17] G. Kresse and J. Hafner, *Phys. Rev. B* **47**, R558 (1993).
- [18] G. Kresse and J. Furthmüller, *Phys. Rev. B* **54**, 11169 (1996).
- [19] S. L. Dudarev, G. A. Botton, S. Y. Savrasov, C. J. Humphreys, and A. P. Sutton, *Phys. Rev. B* **57**, 1505 (1998).
- [20] S. Picozzi *et al.*, *Phys. Rev. B* **75**, 094418 (2007).
- [21] P. E. Blöchl, *Phys. Rev. B* **50**, 17953 (1994); G. Kresse and D. Joubert, *Phys. Rev. B* **59**, 1758 (1999).
- [22] N. A. Pertsev, A. G. Zembilgotov, and A. K. Tagantsev, *Phys. Rev. Lett.* **80**, 1988 (1998).
- [23] R. D. King-Smith and D. Vanderbilt, *Phys. Rev. B* **47**, 1651 (1993).
- [24] J. Samuel Smart, *Effective Field Theories of Magnetism* (Saunders Company, Philadelphia, 1966).
- [25] J. M. Rondinelli, A. S. Eidelson, and N. A. Spaldin, *Phys. Rev. B* **79**, 205119 (2009).
- [26] T. Kimura *et al.*, *Nature* **426**, 55 (2005).
- [27] A. Malashevich and D. Vanderbilt, *Phys. Rev. Lett.* **101**, 037210 (2008).